ELSEVIER

Journal of Molecular Catalysis A: Chemical 135 (1998) 75–88

JOURNAL OF MOLECULAR CATALYSIS A: CHEMICAL

Preparation, characterisation and catalytic behaviour of cobalt–niobia catalysts

V. Pârvulescu [a,*], M. Ruwet [b], P. Grange [b], V.I. Pârvulescu [c]

[a] *Institute of Physical Chemistry, Splaiul Independentei 202, Bucharest 77208, Romania*
[b] *Universite Catholique de Louvain, Unite de Catalyse et Chimie des Materiaux Divises, Place Croix du Sud 2, Louvain-la-Neuve 1348, Belgium*
[c] *University of Bucharest, Faculty of Chemistry, Department of Chemical Technology and Catalysis, B-dul Republicii 13, Bucharest 70346, Romania*

Received 15 July 1997; accepted 26 November 1997

Abstract

Cobalt–niobia catalysts were prepared using the colloidal sol–gel technique. Niobium chloride or niobia oxide were used as precursor. The differences between the procedures used are due to the methods of preparation of the colloidal suspensions and gelification. The catalysts were characterised using adsorption and desorption curves of Kr and N_2 at 77 K, H_2-Chemisorption, XRD, FT-IR, XPS and electron microscopy investigations. Preparation of these catalysts without experimental precautions led to a very inhomogeneous structural and textural material. In contrast, the colloidal sol–gel technique controls both the structure of the niobia oxide and the tailoring of cobalt. A strong metal support interaction effect (SMSI) was present irrespective of the sample preparation variant. Although the rate of butane hydrogenolysis was low for all catalysts, a correlation between TOF and the catalyst crystallite size was found. Selectivity to methane, ethane, propane or to isomerization also depends on the catalyst crystallite size.

Keywords: Cobalt–niobia catalysts; Sol–gel technique; Niobium chloride

1. Introduction

Niobium compounds and niobium-containing materials have been shown to be very useful catalysts, catalyst supports or promoters in various reactions of industrial importance [1–3]. Among the properties that determined the interest for these materials, a few are very important for catalysis: their acidic and redox properties, and also the catalyst life extension obtained when a small amount of niobium oxide is added to known catalysts [1–6]. Niobia was one of the supports examined in order to prove that the reducibility of the support is a key factor in the development of SMSI for metal catalysts subjected to a high-temperature reduction [7]. Later, Ko et al. [8–10], Marcelin et al. [11] Burke and Ko [12], Kunimoro et al. [13–15], Hu et al. [16], Uchijima [17], Frydman et al. [18], Silva et al. [19] and Aranda et al. [20] reported the same

* Corresponding author.

1381-1169/98/$ - see front matter
PII: S1381-1169(97)00287-2

effect using Pt, Rh, Ni and Co as active metals. A few studies deal with alkane hydrogenolysis as a reaction test [12,14,21]. All these experiments indicate that the hydrogenolysis activity of the niobia-supported metals is at least 1×10^4 lower after reduction at high temperatures compared with similar catalysts reduced at low temperatures, because of SMSI effect. The SMSI effect exerted by niobia is similar or higher than that due to titania.

Concerning catalytic reactions, the existence on the surface of different niobium oxides is an important factor in determining the surface reactivity [22]. The niobium–oxygen system can exist in different phases: NbO, NbO_2 and Nb_2O_5 in equilibrium state at room temperature. Nb_2O_5, especially, has many polytypic phases [23].

Many of the techniques used for preparation of acidic niobia or of niobates refer to the sol–gel method [24–28]. According to this method, niobia gels are prepared by mixing niobium ethoxide, butanol, doubly deionized water and an acid. Acetic acid [24], hydrochloric acid [27] or nitric acid are used as acid [25,28]. The gel is then extracted in a standard autoclave with supercritical carbon dioxide to obtain an aerogel, or is treated using typical ageing and drying procedures.

The aim of this study is to investigate the use of the colloidal sol–gel techniques as a tool for controlling the size and the reactivity of the metal in Co/Nb_2O_5 catalysts. To that purpose, niobium alkoxide [29] or niobium chloride were used as precursors. Changing the size of the metal crystallites in this system will probably modify the strength of the SMSI effect. For a better understanding of the impact of the electronic structure on the catalytic activity, data obtained by characterization of the catalysts with different techniques were correlated with catalytic activity data in butane hydrogenolysis, which is a well-known structure-sensitive reaction [30–35]. For this reaction, Coq et al. [32] and Bond et al. [33–35] distinguished between small and large particle behaviours. On small particles, hydrogen is more strongly chemisorbed than on large particles. Small particles exhibit TOF for hydrogenolysis of butane 10–30 times lower than large particles, and large particles show quite different product selectivities as well.

2. Experimental

Five different samples were prepared using niobium chloride or niobium oxide as a precursor. The differences between these samples are mainly due to the procedure used for precipitation of niobium hydroxide in the first step.

(A) $NbCl_5$ was dissolved, in an inert atmosphere, in anhydrous ethanol with generation of a colloidal suspension. Niobium hydroxide was then precipitated under strong stirring, by adding an aqueous Na_2CO_3 solution. After vacuum filtration, the obtained precipitate was peptized with HCl at pH $\cong$ 2. An aqueous $Co(NO_3)_2$ solution was added to the colloidal suspension under stirring. The gelification was carried out in the presence of cobalt at 80°C. Solvent elimination was performed at the same temperature in a rotavapour system.

(B) $NbCl_5$ was dissolved as in (A). The obtained suspension was vigourously stirred, then water was added under controlled flow, in order to generate a gelatinous precipitate. The precipitate was then peptized in the presence of HCl. An aqueous $Co(NO_3)_2$ solution was added under continuous stirring to the colloidal suspension obtained as described above. Gel formation and solvent elimination were performed as in (A).

(C) Gelification was performed without previous niobium hydroxide precipitation. First, $NbCl_5$ was dissolved in CCl_4 under an inert atmosphere. A very stable colloidal suspension was obtained after anhydrous ethanol addition. Then, the pH was modified to 1 by adding HCl and the formation of the sol began. $Co(NO_3)_2$ in alcoholic solution was added during the sol formation. Subsequently, PEG 6000 in $C_2H_4Cl_2$ was added. Under these conditions, part of the

cobalt passed into the organic phase. After elimination of a small quantity of solvent, the temperature was increased to 60°C, and the gelification process started; solvent elimination was performed like in the first case.

(D) In this procedure, CBMM–Nb_2O_5 (Companhia Brasiliera de Metalurgia e Mineracao, with a surface area of 95 $m^2\ g^{-1}$) was peptized directly with HCl at pH 1.5 under strong agitation and refluxation. The process was very slow and required a long time (about 5–6 days). A solution of $Co(NO_3)_2$ was added to the resulting colloidal suspension, under agitation. Solvent elimination was performed as in (A).

(E) A Co/Nb_2O_5 sample obtained by wet impregnation technique of CBMM–Nb_2O_5, using $Co(NO_3)_2$, was also prepared for comparison.

All samples were then reduced in a flow of 30 ml min^{-1} hydrogen at 823 K for 8 h. The above catalysts were characterised using several techniques.

Elemental analysis of the samples was performed by atomic emission spectroscopy with inductively coupled plasma atomization (ICP-AES) after drying of the samples overnight at 100°C (Table 1). Adsorption and desorption curves of Kr and N_2 at 77 K were obtained with a Micromeritics ASAP 2000 apparatus after degassing the samples at 150°C under vacuum. This allowed to determine the surface area and the pore volume of the samples (Table 1).

H_2-Chemisorption was carried out using a Micromeritics ASAP 2010C. Reduced samples were evacuated, first at 393 K and then at 723 K. In a second step, a hydrogen flow was passed initially at 308 K for 15 min and then at 723 K for 120 min. After reduction, the samples were purged with a helium flow at 690 K for 120 min and then at 308 K for another 30 min. Adsorption isotherms were measured at 308 K by the desorption method after a 45-min equilibration at 300 Torr of adsorbate. The total gas uptake was determined by extrapolating the straight-line portion of the adsorption isotherm to zero pressure. Reversible H_2 uptakes were measured by evacuating to 5×10^{-5} Torr and the adsorption temperature, and measuring a second isotherm. The irreversible uptake was determined from the difference between the total gas uptake and reversible uptake. The cobalt dispersion, cobalt surface area and the crystallite metallic size were determined using the irreversible uptake and assuming a 1:1 H:Co surface stoichiometry [36–38]. The quantity of metal considered in these measurements was that determined using O_2 titration. These experiments were performed using reduced catalysts at 823 K in conditions of TPO. In such respect, it used a Micromeritics PulseChemisorb 2705 apparatus in the presence of 50 ml min^{-1} O_2 (5%)—He flow. Typical experiments were carried out at 723 K by increasing the temperature with 10 K min^{-1}. Reduced cobalt was determined assuming that it passes at 723 K into Co_3O_4 [39]. This assumption was confirmed also by XRD and XPS. The actual fraction of Co was used to determine the metal dispersions

Table 1
Chemical composition and textural characteristics of the investigated samples

Route of preparation	Chemical composition (wt.% Co)	Chlorine content (wt.%)	Surface area ($m^2\ g^{-1}$)	Pore volume ($cm^3\ g^{-1}$)
CBMM–Nb_2O_5	0	0	68	3.45
Route A	9.99	0.19	17[a]	3.04[a]
Route B	9.89	0.19	38[a]	4.68[a]
Route C	9.94	0.19	57	4.63
Route D	10.11	0.19	12[a]	1.57[a]
Route E	10.15	0	6.56[a]	1.16[a]

[a] Determined using Kr.

and then to calculate the density of exposed metal atoms and to report reaction rates as turnover rates.

XPS spectra were recorded using a SSI X probe FISONS spectrometer (SSX-100/206) with monochromatic Al Kα radiation. The energy scale was calibrated using the Au $4f_{7/2}$ peak (binding energy 93.98 eV). With the analyser energy used (50 eV), the full width at half maximum of $4f_{7/2}$ peak was 10 eV. The samples were moderately heated by a quartz lamp in the introduction chamber of the spectrometer to promote degassing, thus improving the vacuum in the analysis chamber. Vacuum in the analysis chamber during analysis was 1×10^{-9}–1×10^{-10} Pa. For calculation of the binding energies, the peaks of the C–(C,H) component coming from carbon contamination (284.8 eV) were used as an internal standard. The composite peaks were decomposed by a fitting routine included in the ESCA 8.3 D manufacturer software. The superficial composition of the investigated samples was analysed using the same software. To avoid the oxidation of the reduced samples, their transfer from the microreactor where they were reduced to the XPS apparatus was made under isooctane. It was followed by bands assigned to $Co_{3p3/2}$, $Nb_{3d5/2}$ and O_{1s}, respectively.

FTIR spectra were recorded with a Bruker IF 88 spectrometer. Self-supported wafers (15 mg cm^{-2}) prepared using KBr were used. Spectra were collected from the accumulation of 16 scans at 1 cm^{-1} resolution.

Samples for electron microscopy investigations were obtained using the following procedure. The samples were dispersed in water with an ultrasonic vibrator. A drop of the resulting suspensions was deposited on a thin carbon film supported on a standard copper grid. After drying, the samples were observed and analysed by TEM method on an JEOL-JEM 200 CX Temscan electron microscope with a resolution of 0.35 nm. The accelerating potential used was 200 kV. The apparatus is equipped with a Kewex energy dispersive spectrometer for electron probe microanalysis (EXD). Each position was investigated in at least 25 points.

XRD measurements of the samples were made with a SIEMENS D-5000 (Θ–Θ) diffractometer of power of 40–50 mA, and equipped with a variable slit, diffracted beam monochromator, and scintillation counter. The diffractograms were recorded in the range 2Θ: (0–80°) with a speed of 0.5° min^{-1} using CuKα radiation ($\lambda = 1.5418$ Å).

Butane hydrogenolysis was carried out in a quartz microreactor connected online to a Carlo–Erba gas chromatograph by a glass trap and a sampling valve. The pressure inside the microreactor was atmospheric and the hydrogen-to-butane ratio was 10:1. Reactants and products were analysed using a flame-ionisation detector, and were separated on a 6-m column containing Chromosorb W coated with silicon oil. Evolution of the reaction was followed by the decrease of the concentration of the reactant expressed as a percentage of the total carbon. Each experiment used 0.3 g catalyst. Reaction rates are expressed as a mmole alkane reacted, (g^{-1} Co) h^{-1}. The selectivity of product j was defined using Bond's formula [33,34]: $S_j = c_j/A$, where c_j is the molar fraction of products containing j carbon atoms ($j < 4$), and A the number of moles converted. The isomerisation selectivity is the fraction of *n*-butane converted to isobutane. Data were recorded using clean catalysts in the first 5 min of reaction. This allowed to control the modification of the kinetic parameters due to the deactivation by carbon deposition. Long-time experiments to determine the stability of the catalysts were also performed. The experiments were carried out in the temperature range 473–673 K. The increase of the temperature to the working conditions was performed at a rate of 2 K min^{-1}. The alkane flow was kept constant at 30 ml min^{-1}. In the investigated conditions, the conversions were below 15%. Hydrogen was purified through a Deoxo catalytic purifier and two traps (silica gel and zeolite 13 X). Butane purity was higher than 99.95%. Before reaction, butane

was passed through a trap containing zeolite 4A.

3. Results

3.1. XRD investigation

The XRD patterns shown in Fig. 1 indicate a well-crystallized structure for samples A and E only. The other samples exhibit an amorphous structure irrespective of the preparation variant. Analysis of these patterns considering ASTM references show different compositions according to the preparation method.

Sample A, obtained via a procedure that is not a typical sol–gel one, contains two kinds of Nb_2O_5 (ASTM 37-1468 (monoclinic) and ASTM 5-0352), some monoclinic NbO_2 (ASTM 19-0859) and orthorhombic $CoNb_2O_6$. The other two samples obtained via $NbCl_5$ using a more usual sol–gel procedure exhibit amorphous features. In these cases, for sample B, XRD indicates the presence of monoclinic Nb_2O_5 (ASTM 19-0862) and monoclinic $Nb_{12}O_{29}$. Lines of orthorhombic $CoNb_2O_6$ (ASTM 32-0304) were also found. A similar structure was also found for sample C. Lines of Nb_2O_5 (ASTM 5-0352) and $NbO_{2.46}$ (ASTM 23-0447), as well as of orthorhombic $CoNb_2O_6$ (ASTM 32-0304) were found. Samples obtained via Nb_2O_5 (sample D) also exhibit amorphous features. XRD analysis indicates the existence of Nb_2O_5 (ASTM 32-0710) and cubic Co_3O_4 (ASTM 9-0418), but also of $Co_4Nb_2O_9$ (ASTM 38-1457). Samples obtained by impregnation of niobia contain Nb_2O_5 (ASTM 37-1468 and ASTM 5-0352), $CoNb_2O_6$ (ASTM 32-0304) and Co_3O_4 (ASTM 9-0418). A small extent of monoclinic NbO_2 (ASTM 19-0859) is also included.

After reduction in hydrogen, samples A and E preserve their crystallinity (Fig. 2). Under these conditions, sample B becomes crystalline as well. The phase composition of these samples changed during treatment in hydrogen. Thus, sample A contains in addition, a reduced phase $Co_{0.97}Nb_{0.03}$. After reduction, sample B

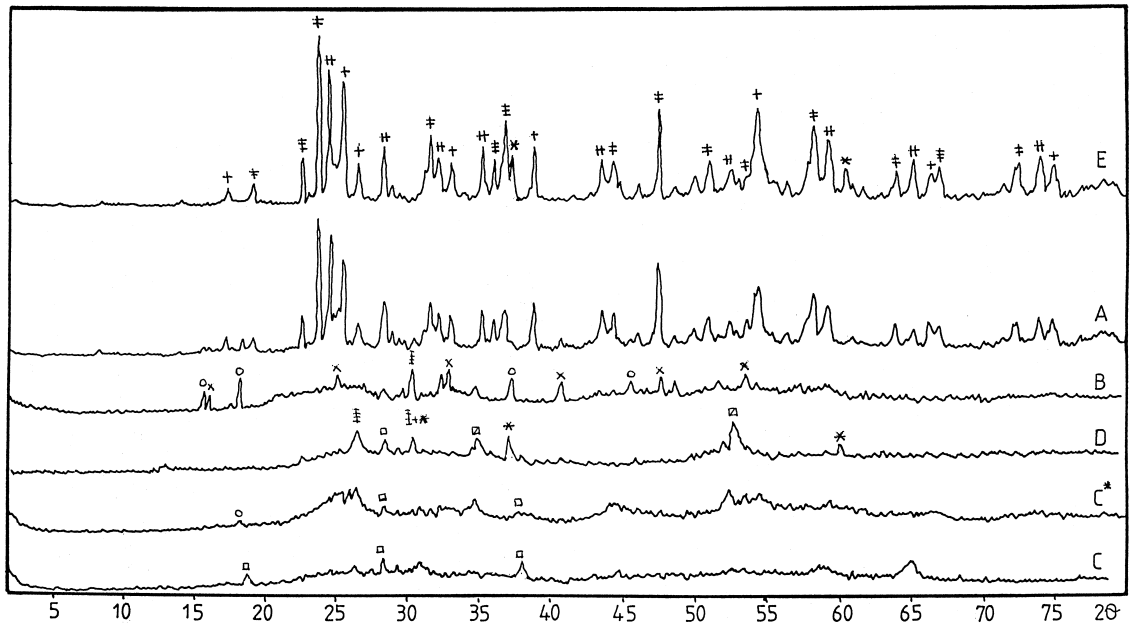

Fig. 1. XRD patterns of the dried Co–Nb_2O_5 samples. C*: calcined at 823 K. ‡: Nb_2O_5 (ASTM 37-1468); †: Nb_2O_5 (ASTM 5-0352); four short horizontal lines on a vertical line: Nb_2O_5 (ASTM 32-0710); ×: Nb_2O_5 (ASTM 19-0862); □: $NbO_{2.46}$ (ASTM 23-0447); ○: $Nb_{12}O_{29}$ (ASTM 16-0734); three short horizontal lines on a vertical line: NbO_2 (ASTM 19-0859); ∗: Co_3O_4 (ASTM 9-0418); a short horizontal line on two vertical lines: $CoNb_2O_6$ (ASTM 32-0304); box with diagonal line: $Co_4Nb_2O_9$ (ASTM 38-1457).

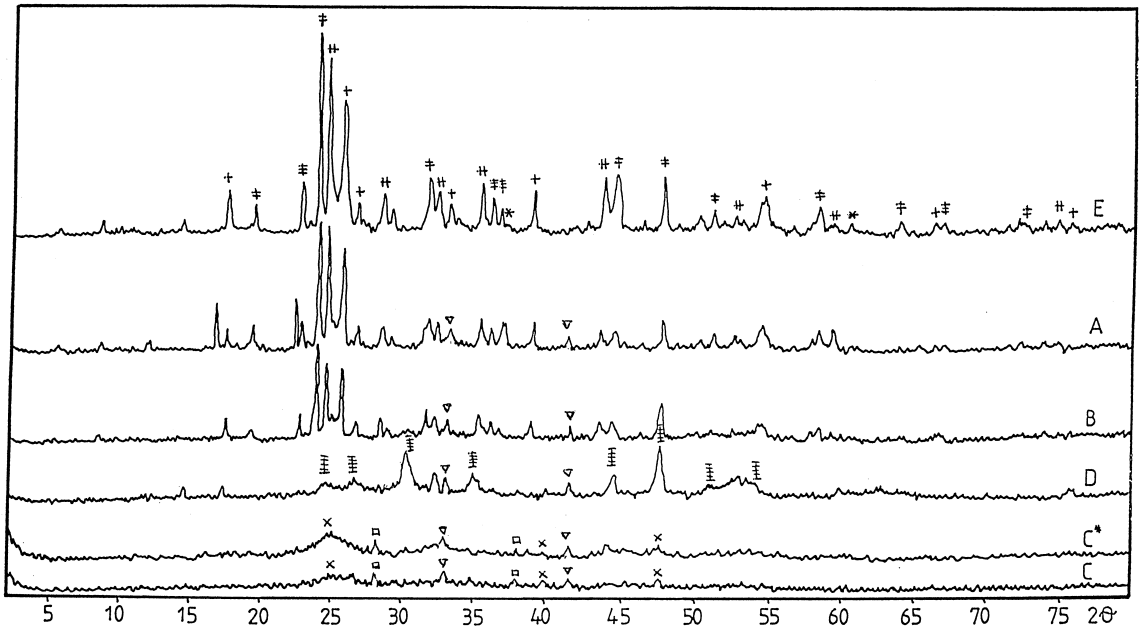

Fig. 2. XRD patterns of the reduced Co–Nb_2O_5 samples. C*: calcined at 823 K and then reduced. ‡: Nb_2O_5 (ASTM 37-1468); †: Nb_2O_5 (ASTM 5-0352); four short horizontal lines on a vertical line: Nb_2O_5 (ASTM 32-0710); ×: Nb_2O_5 (ASTM 19 0862); five short horizontal lines on a vertical line: Nb_2O_5 (ASTM 16-0053); □: $NbO_{2.46}$ (ASTM 23-0447); ○: $Nb_{12}O_{29}$ (ASTM 16-0734); three short horizontal lines on a vertical line: NbO_2 (ASTM 19-0859); ∗: Co_3O_4 (ASTM 9-0418); a short horizontal line on two vertical lines: $CoNb_2O_6$ (ASTM 32-0304); box with diagonal line: $Co_4Nb_2O_9$ (ASTM 38-1457); ▽: $Co_{0.97}Nb_{0.03}$ (ASTM 23-0459).

exhibited a phase composition very close of those found for sample A. Sample C contains monoclinic Nb_2O_5 (ASTM 19-0862), $NbO_{2.46}$ (ASTM 23-0447) and a reduced phase $Co_{0.97}Nb_{0.03}$ (ASTM 15-0459). Sample D, obtained via Nb_2O_5, also contains Nb_2O_5, but in the forms corresponding to ASTM 32-0710 and ASTM 16-0053, and $Co_{0.97}Nb_{0.03}$. In the case of the sample obtained by impregnation, like in the case of sample A, the phase composition was very close of those in the non-reduced sample, but the crystallinity was a little bit diminished.

3.2. Skeletal FT-IR spectra

FT-IR spectra in the lattice vibration range of the reduced samples are shown in Fig. 3. The shape of these spectra depends on the preparation variant of the samples. Spectra of the samples prepared via the sol–gel method (B, C and D) contain only few bands: at 498, 600 and 679 cm^{-1} for sample B, at 517, 573 and 597 cm^{-1} for sample C and at 570, 600 and 678 cm^{-1} for sample D. They could be assigned to deformation vibrations (495–520 cm^{-1}), symmetric stretching (673–698 cm^{-1}) or to some vibrations of secondary building units (570–570 cm^{-1}). In contrast, the spectra of sample A and that obtained by impregnation (E) contain several additional bands (sample A at 491, 557, 594, 663, 745, 824 and 958 cm^{-1} and sample E at 491, 576, 663, 745, 833 and 959 cm^{-1}). This situation could be correlated with the number of phases found in XRD analysis and, in consequence, indicates a more heterogeneous structure. In the case of the samples prepared via sol–gel, cobalt can enter in niobia octahedral entities having features similar to these. In such a way, one can explain why the FT-IR spectra of samples B, C and D exhibit only few bands. The XRD pattern indicates that after reduction of the samples A and E, some lines disappeared. But the presence of these supplementary IR

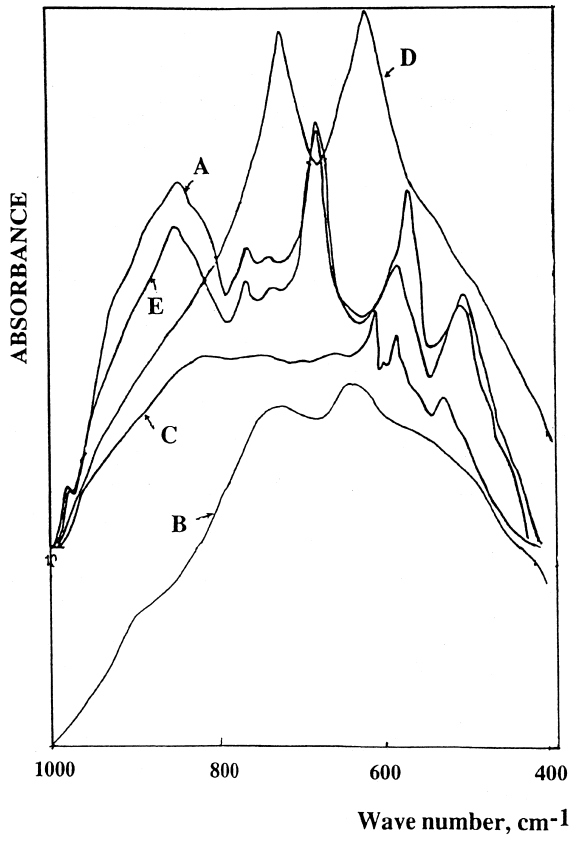

Fig. 3. Skeletal FT-IR spectra of the reduced Co–Nb_2O_5 samples.

bands in the spectra recorded for the reduced samples seems to indicate that only a partial reduction of these occurs.

3.3. H_2 chemisorption

The results of the chemisorption measurements are given in Table 2. The degree of reduction determined for these samples is rather low. The SMSI effect does not induce, inevitably, a lower reduction degree of the metal, but in this case it is very probable that low values determined for the reduction degree are also related with this effect [37,40]. Sample C also has a low reduction degree, maybe correlated with the homogeneity exhibited by this sample, and has a cobalt dispersion that is generally achieved by impregnation of small metal contents, or in the presence of the supports that interact very weakly with the metals [37]. Pure $CoNb_2O_6$ was found to exhibit zero H_2 uptake.

3.4. TEM analysis

Figs. 4–8 show the topography of the investigated catalysts and the homogeneity of the cobalt distribution on the niobia support. Impregnation (sample E (Fig. 8)), also the variant A (Fig. 4) lead to cobalt agglomeration on the catalyst surface, and to an evident non-homogeneity of the surface composition. On the contrary, samples B (Fig. 5), D (Fig. 6) and more evidently, sample C (Fig. 7), exhibit a large homogeneity of the surface composition (i.e., a narrow distribution of the cobalt-to-niobia ratio). In the latter, this ratio is within the limits 0.35–0.6. A reduced cobalt size is evidently a consequence of the surface homogeneity. Very good concordance with the H_2 chemisorption was obtained. Thus, sample E (Fig. 8) showed agglomerates of well crystallized grains larger than 100 Å; for sample C (Fig. 7), the dimension of the metallic

Table 2
Hydrogen uptake, metal dispersion, metal surface area and crystallite metal size of Co–Nb_2O_5 catalysts

Catalyst	Degree of reduction[a] (%)	H_2 uptake (μmol g_{cat}^{-1})	Cobalt dispersion (%)	Metal surface area (m^2 g^{-1})	Crystallite size	
					H_2 chemisorption	TEM
Sample A	6.3	14.5	13.5	0.58	71	60–95
Sample B	5.1	23.2	26.7	0.92	36	30–50
Sample C	4.2	26.3	37.3	1.05	26	25–30
Sample D	6.0	15.1	14.9	0.60	64	50–70
Sample E	6.8	7.1	6.2	0.28	153	> 100

[a] Determined by O_2 titration assuming that the reduced cobalt is oxidated at Co_3O_4.

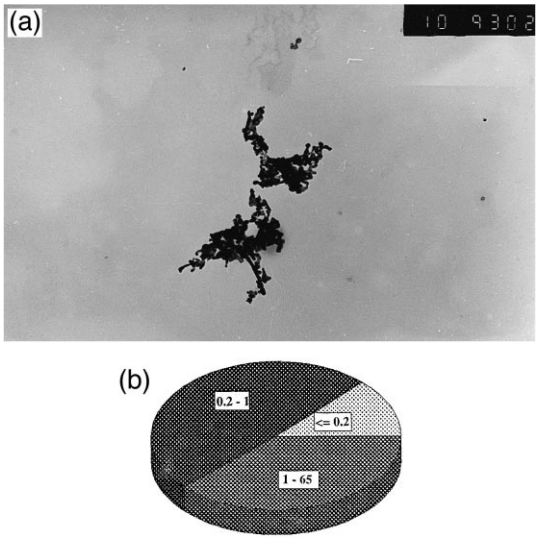

Fig. 4. Topography (a) and superficial distribution (b) of Co:Nb ratio for sample A. 1 cm = 0.07 μ.

cobalt is in the range 25–30 Å, between 30–50 Å for sample B (Fig. 5) and 50–70 Å for sample D (Fig. 6) and in a quite large interval 60–95 Å for sample A (Fig. 4).

3.5. XPS

XPS parameters of the recorded spectra for both the dried and reduced A–E catalysts are presented in Table 3. Deposition of cobalt as Co^{2+} salt results in the formation of three main Co species: bulk Co_3O_4, Co^{2+} ions in tetrahedral sites (surface like-spinels) and Co^{2+} ions in octahedral sites. The assignment of these species resulted from the deconvolution of the $Co_{3p3/2}$ band. The relative distribution of these species on the surface is generally dependent on the

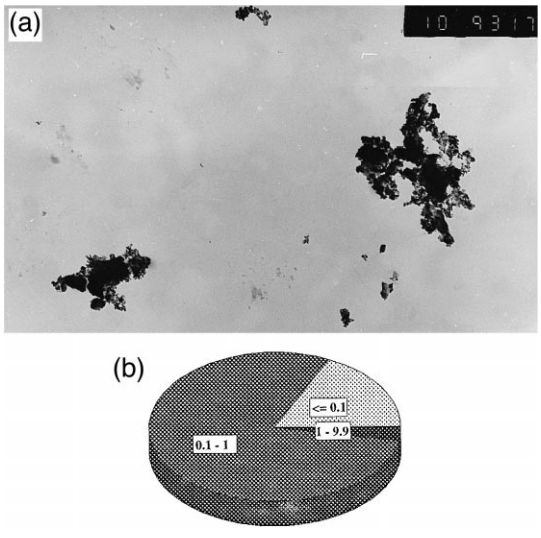

Fig. 5. Topography (a) and superficial distribution (b) of Co:Nb ratio for sample B. 1 cm = 0.20 μ.

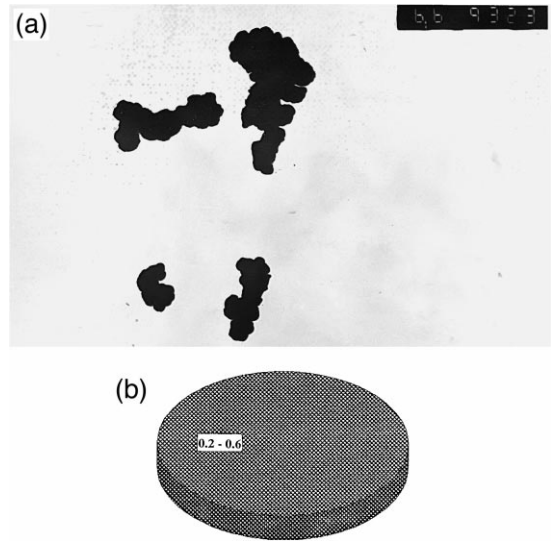

Fig. 6. Topography (a) and superficial distribution (b) of Co:Nb ratio for sample C. 1 cm = 0.035 μ.

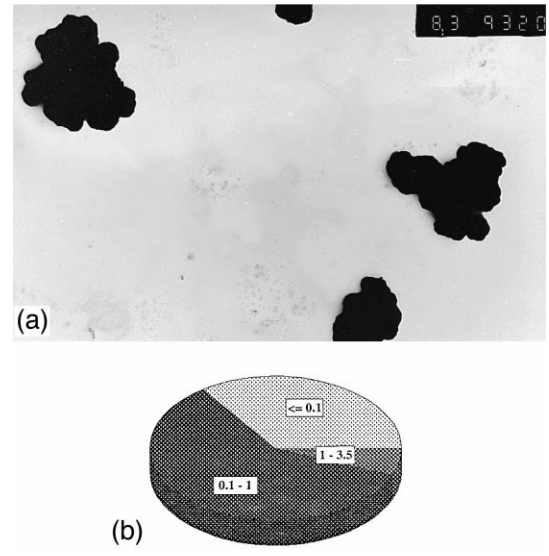

Fig. 7. Topography (a) and superficial distribution (b) of Co:Nb ratio for sample D. 1 cm = 0.17 μ.

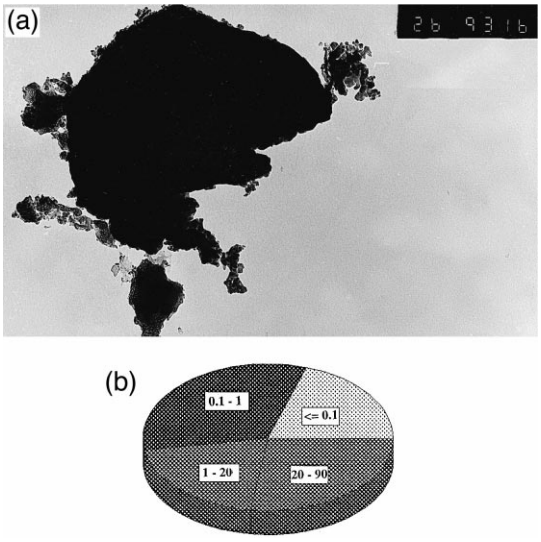

Fig. 8. Topography (a) and superficial distribution (b) of Co:Nb ratio for sample E. 1 cm = 0.15 μ.

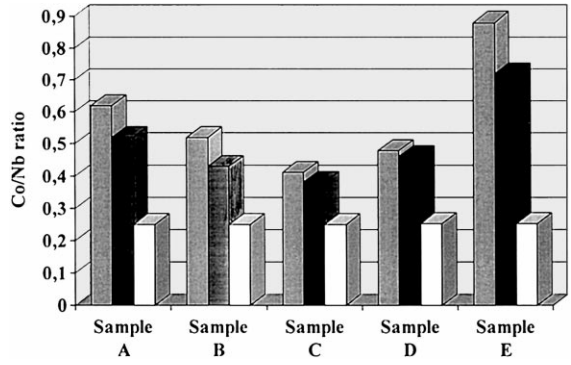

Fig. 9. Evolution of the Co:Nb ratio determined from XPS for the dried (lightly shaded box) and reduced samples (■) comparatively with the chemical composition (□).

cobalt content and calcination temperature. High Co concentrations typically form a phase consisting of Co_3O_4 crystallites that can be easily reduced. Species Co^{2+} in tetrahedral positions, as well as those in octahedral sites are difficult to reduce.

All dried catalysts contain Co^{2+} species in tetrahedral, as well as octahedral positions. Furthermore, the XPS spectra of samples A, D and E exhibit binding energies typical for Co_3O_4. The binding energies of the main $Co_{3p3/2}$ line correspond to a more oxidized Co^{2+} than that corresponding to $CoNb_2O_6$ that is located around 780.5 eV. After reduction, the $Co_{3p3/2}$ peak of Co_3O_4 disappears, but another one corresponding to reduced cobalt appears, irrespective of the variant through which were prepared the samples. In the samples obtained via the sol–gel technique, the binding energies are located at higher values than that of metallic cobalt or even that reported by Stranick et al. [41] for Co/Al_2O_3 catalysts. This could suggest the presence of a SMSI effect. When compared to the chemical composition of the samples evolution of the XPS Co:Nb ratios for the dried and reduced samples show that, after reduction, a

Table 3
XPS parameters of the dried and reduced catalysts

Catalyst	O_{1s}	$Nb_{3d5/2}$	$Nb_{3d3/2}$	$Co_{3p3/2}$ reduced	$Co_{3p3/2}$ (Co_3O_4)	$Co_{3p3/2}$ main	$Co_{3p3/2}$ $CoNb_2O_6$ satellite
Dried							
A	530.1	207.1	209.8	–	779.3	782.9	787.4
B	530.1	207.0	209.8	–	–	781.0	785.9
C	530.3	207.2	209.9	–	–	781.1	786.1
D	530.0	206.8	209.5	–	779.1	782.4	787.8
E	530.1	207.2	209.9	–	779.2	780.8	786.3
Reduced							
A	530.0	207.1	209.8	778.0	–	782.7	787.5
B	530.2	207.0	209.8	778.3	–	781.2	786.1
C	530.3	207.2	209.9	778.6	–	781.4	786.1
D	530.2	206.8	209.5	778.2	–	782.1	786.2
E	530.0	207.2	209.9	777.9	–	781.0	787.1

Table 4
Kinetic parameters for *n*-butane hydrogenolysis

Catalyst	Temperature range (K)	Rate (mmol g Co^{-1} h^{-1})	TOF (h^{-1})	Preexponential factor	Activation energy (kJ mol^{-1})
Sample A	523–573	0.7	3.1	7.1×10^{14}	149.7
	573–623	9.2	40.2	7.9×10^{14}	150.9
	623–673	219.3	957.3	2.1×10^{15}	154.5
Sample B	523–573	0.8	1.8	1.2×10^{14}	141.2
	573–623	9.2	20.3	1.3×10^{14}	142.5
	623–673	175.5	387.4	2.1×10^{14}	143.5
Sample C	523–573	0.9	1.4	2.8×10^{13}	133.9
	573–623	8.7	13.7	1.9×10^{13}	135.0
	623–673	136.4	215.5	3.9×10^{13}	136.2
Sample D	523–573	0.8	3.2	2.9×10^{14}	145.3
	573–623	9.4	37.2	2.4×10^{14}	146.6
	623–673	194.4	768.9	5.1×10^{14}	147.6
Sample E	523–573	0.6	5.7	1.2×10^{16}	162.8
	573–623	8.9	84.6	8.7×10^{15}	163.8
	623–673	261.8	2488.5	1.9×10^{16}	164.7

Rate is given for 523, 573 and 623 K; TOF was calculated as mmol $mol_{Co^{-1}}$ h^{-1} D^{-1} where D is the dispersion. TOF was calculated for conversions of 14%.

small increase of this ratio occurs, again irrespective of the sample preparation variant (Fig. 9).

3.6. Butane hydrogenolysis

The rate of butane hydrogenolysis was low irrespective of the preparation variant of the catalysts (Table 4). However, differences between the catalysts were evident. TOF values make these differences more evident. It appears that the catalysts with a lower dispersion degree (sample E) exhibit higher activities, whereas the low TOF values were recorded on catalysts with a higher dispersion degree (sample C).

Satisfactorily, linear Arrhenius plots based on the rate of reactant removal were obtained for all catalysts in each stage (Table 4). Inspection

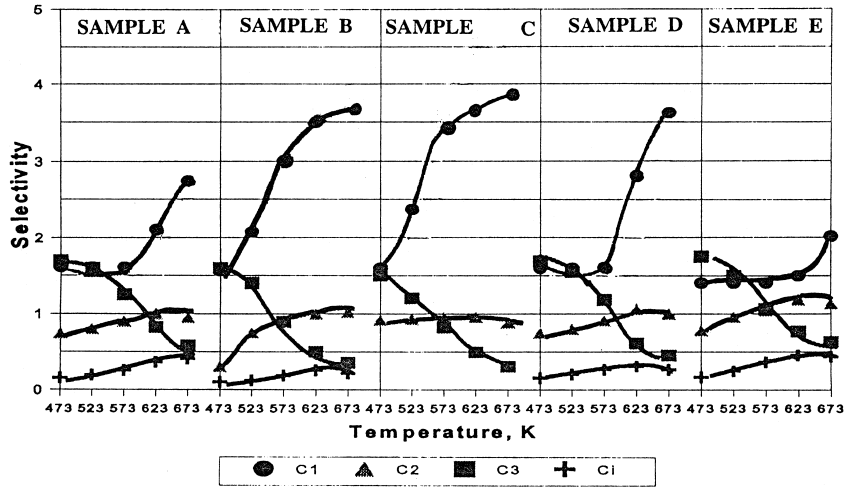

Fig. 10. Variation of the selectivity with the temperature and catalysts nature. Selectivity of product j was defined using Bond's formula: $S_j = c_j/A$, where c_j is the molar fraction of products containing j carbon atoms ($j < 4$), and A the number of moles converted.

of the Arrhenius energies showed that *n*-butane hydrogenolysis exhibits a lower activation energy on catalyst C and a higher one on the impregnated Co/Nb_2O_5 catalyst. This change in the apparent activation energy does not inevitably mean that on the catalyst C reaction occurs through more adsorption steps, but indicate changes in the values of the rate and adsorption constants [31–33].

It is noteworthy that the activities of catalysts B, D and furthermore that of sample C were fairly stable in time. In contrast, in the case of sample A and even more for sample E, butane hydrogenolysis underwent a certain deactivation. The decay in the reaction rate after 30 min was about 32% for sample A and 43% for sample E.

The selectivity towards methane exhibits a maximum for sample C, which has the highest dispersion and homogeneity of the Co:Nb ratio. On the same catalyst, the isomerisation selectivity is zero, irrespective of the reaction temperature. The selectivity towards propane decreases at high temperature, and high dispersions (samples B and C) favour a further decrease. Selectivity to ethane except low temperatures, and sample E do not differ very much. Selectivity to isobutane exhibits similar features to that of ethane (Fig. 10).

4. Discussion

Impregnation of the niobia with a high loading of Co (sample E) leads to a strong decrease of the surface area. The XRD patterns also indicate a crystalline structure after reduction with hydrogen. Under these conditions, niobia co-exists in two forms (ASTM 37-1468 and ASTM 5-0352). During reduction, most of the Co_3O_4 becomes reduced to cobalt, which, as shown by H_2-Chemisorption and TEM, exists as large crystalline grains, non-homogeneously dispersed on the niobia surface. TPO shows that 6% Co is under the form Co_3O_4, i.e., Co^0 ($d_p = 15$ nm) after reduction, and XPS shows that the rest is as Co^{2+} and enriched the surface layers. In this case, we totally agree with the recent model of Frydman et al. [42], who supposed that the surface of niobia is covered by a homogeneous layer of Co^{2+} and islands of reduced Co.

Samples prepared by variant A exhibit features that are close to those of samples prepared via impregnation. Thus, the dimension of the reduced cobalt is also large, and the non-homogeneity of the superficial Co:Nb ratio is still high. Sample A also preserves its crystallinity after reduction. A larger homogeneity of the Co:Nb ratio was achieved in cases B and D by modifying the route of the sol–gel procedure. Moreover, some intrinsic characteristics were changed as FT-IR showed, leading to amorphous-like structures. The behaviour of the sample obtained via route C is noteworthy: it appears that the diminishing of the cobalt size favours not only a homogeneous distribution of cobalt in niobia, but also its penetration in the niobia structure. This behaviour is facilitated by the PEG 6000 presence. Therefore, one can suppose that the subsequent addition of the PEG 6000 in $C_2H_2Cl_2$ avoids the agglomeration of cobalt, determining its dispersion in the niobia matrices.

O_2-titration of the reduced samples, except sample C and partially B, indicates rather small differences among the catalysts. On the contrary, H_2-chemisorption data indicate large differences. The dispersion determined for sample C is not very usual, being typical for low concentration of cobalt or for the supports that allow a high reduction degree like carbon [37]. On the other hand, it is true that the reduced Co, i.e., Co^0, in this case concerns only 4.2% of the 9.94 wt.% Co in this sample.

XPS data suggest the presence of a SMSI effect between cobalt and niobia for all the samples. This effect is more important in the case of catalyst C that contains smaller cobalt particles with a more homogeneous distribution in niobia. Because of the niobia features, i.e., the capacity to lose oxygen and to pass in a

reduced state, SMSI between cobalt and niobia is independent of the preparation variant. Niobia is well known as an oxide which exists in a polymorphic state [23]. In the presence of a metal, the structure of the support becomes more complex because a small part of it, due to the SMSI effect, transforms to a reduced NbO_x ($x < 2.5$) form and another one to a niobate like compound. The use of the colloidal sol–gel technique can preclude the formation of multiple niobia phases and can tailor the size and the shape of the dispersed metal islands. In a similar way, using the colloidal sol–gel technique, the surface area can be substantially increased as compared to impregnated catalysts. Using modified variants, different surface areas and metal sizes from those obtained by a pure sol–gel technique and impregnation can be achieved.

XPS data led us to suppose that SMSI effect appears as a concerted contribution of a crowning effect of niobia on the Co surface and of an electronic effect. The crowning effect could be appreciated from the higher XPS Nb:Co ratio in the case of the samples B, C and D. The same effect could not be supposed in the case of samples A and E. The second one is related with the presence of strong acid sites in niobia that could exert a strong influence upon the cobalt neighbour atoms. Therefore, according to the cobalt dispersion and the niobia phase composition one can suppose a different intensity of this effect.

Our model differs on the classical view of SMSI effect, in which the migration, and in consequence the decoration of TiO_x moieties onto Pt particles occurs. As we already mentioned, in our case SMSI is a consequence of the contribution of a crowning effect of niobia on the Co surface. XPS and even more TEM results led us to such a conclusion.

The SMSI effect of niobia-supported metal catalysts in hydrogenolysis has been recently proved by Brown and Kemball [21]. They showed that the SMSI effect leads to a reduction in the rate of hydrogenolysis, and that effects of SMSI would have been even more marked if the catalysts had been more highly dispersed. This assumption was also verified in our series of catalysts. The TOF measured for catalyst E is 10 times higher than that determined for catalyst C.

However, it seems that the determinant factor in hydrogenolysis is not the SMSI, but the effect of the crystallite size. Differences determined between the investigated catalysts are mainly due to the differences in the latter parameter. This conclusion concords very well with recent results of Coq et al. [32], Bond et al. [31,33–35] and Ponec and Bond [43], and is supported by the fact that, in our case no decoration but only crowning of the active species occurs.

In addition to these factors, Ponec and Bond [43] pointed out that the presence of toxins from the precursors like Cl^- could also exhibit a negative effect. Chlorine content was in the same range for catalysts A–D; therefore, one can suppose that its influence is related to that of the SMSI exerted by niobia. On the contrary, in the case of catalyst E, the absence of chlorine and of the crowning contribution of niobia correlated with large metal particles could also explain the TOF determined on this catalysts.

Previous studies indicated that in *n*-butane hydrogenolysis, the effect of the support is far from being an inert one. Thus, Yoshitake et al. [44] proved that niobia on peripheral NbO_x islands could adsorb both hydrogen and alkenes. Other authors such as Gallezot et al. [45] and Torok et al. [46,47] indicated the possibility that dehydrogenated species spillover to the support.

As we already mentioned, the determination of the reaction rates in *n*-butane hydrogenolysis shows that dispersion plays a more important role. It is also possible that dehydrogenated species located at the boundary of small particles have a beneficial effect. The acidic properties of niobia could hinder the self-poisoning of the active sites by the surface reaction products, and this behaviour could be facilitated by small metal particles. In these cases, the contact between the active metals and the crown niobia

support is increased, and we can speculate that species that could polymerise are trapped by the acidic sites of the support. In such a way, one can explain the higher stability of catalyst C compared with E. The differences in TOF alone could not explain their different stability.

The differences in selectivity are also a consequence of the variation of the particle size. Cobalt dispersion influences the distribution of the *n*-butane hydrogenolysis products. One can just notice the behaviour of catalyst C on which isobutane has not been identified, and where selectivity to methane has the highest values. The isomerisation selectivity is zero, irrespective of the reaction temperature. As it was shown above, the selectivity towards methane exhibits a maximum for sample C, which has the highest dispersion and the highest homogeneity of the Co:Nb ratio. The selectivity towards propane decreases at high temperature, and high dispersions (samples B and C) favour a further decrease. Selectivity to ethane, except at low temperatures, and sample E does not differ very much. Selectivity to isobutane exhibits similar features with that of ethane.

5. Conclusions

The use of the colloidal sol–gel technique offers a tool to control both the structure of niobia and the homogeneity of a complex system like cobalt–niobia. Using such a route, it is possible to control the dimension of cobalt and also the cobalt:niobium ratio.

Reduction of the catalysts in hydrogen at 823 K leads to the appearance of an SMSI effect that depends on the size of the cobalt particles and on the structure of niobia. Due to this effect, butane hydrogenolysis occurs with low reaction rates, irrespective of the variant of preparation of the catalyst. However, the determinant factor in the TOF values seems to be the metallic crystallite size, as it was already mentioned in the literature. At the same time, both the selectivity to hydrogenolysis and to isomerisation are influenced by the same parameter.

References

[1] K. Tanabe, Catal. Today 8 (1990) 1.
[2] K. Tanabe, Chem. Technol. 21 (1991) 628.
[3] K. Tanabe, S. Okazaki, Appl. Catal. A 133 (1995) 191.
[4] P. Carniti, A. Gervasini, A. Auroux, J. Catal. 150 (1994) 274.
[5] P. Batamack, R. Vincent, J. Fraissard, Catal. Lett. 36 (1996) 81.
[6] J.C. Vedrine, G. Coudurier, A. Ouqour, P.G.P. de Oliveira, J.C. Volta, Catal. Today 28 (1996) 3.
[7] S.J. Tauster, S.C. Fung, J. Catal. 55 (1978) 29.
[8] E.I. Ko, J.M. Hupp, F.H. Rogand, N.J. Wagner, J. Catal. 84 (1983) 85.
[9] E.I. Ko, J.M. Hupp, N.J. Wagner, J. Catal. 86 (1984) 315.
[10] E.I. Ko, R. Bafrali, N.T. Hufher, N.J. Wagner, J. Catal. 95 (1985) 260.
[11] G. Marcelin, E.I. Ko, J. Lester, J. Catal. 96 (1985) 202.
[12] P.A. Burke, E.I. Ko, J. Catal. 116 (1989) 230.
[13] K. Kunimoro, H. Abe, E. Yamaguki, S. Matsui, T. Uchijima, Proc. 8th Int. Congr. Catal., Vol. 5, Dechema, Frankfurt am Main, 1984, p. 251.
[14] K. Kunimoro, K. Ito, K. Iwai, T. Uchijima, Chem. Lett. 573 (1986) .
[15] K. Kunimoro, Y. Doi, K. Ito, T. Uchijima, J. Chem. Soc., Chem. Commun. (1986) 965.
[16] Z. Hu, H. Nakamura, K. Kunimoro, H. Asano, T. Uchijima, J. Catal. 112 (1988) 478.
[17] T. Uchijima, Catal. Today 28 (1996) 105.
[18] A. Frydman, R.R. Soares, M. Schmal, in: L. Guczi, F. Solymosi, P. Tetenyi (Eds.), New Frontiers in Catalysis, Proc. 10th Int. Congr. Catal., Part C, Akabemiai Kiado, Budapest, 1992, p. 2797.
[19] R.R.C.M. Silva, M. Schmal, R. Frety, J.A. Dalmon, J. Chem. Soc., Faraday Trans. 89 (1993) 3795.
[20] D.A.G. Aranda, A.L.D. Ramos, F.B. Passos, M. Schmal, Catal. Today 28 (1996) 105.
[21] R. Brown, Ch. Kemball, J. Chem. Soc., Faraday Trans. 92 (1996) 281.
[22] K. Obara, K. Iwasaki, S. Matushima, T. Hirose, M. Shiroga, Y. Suemoto, Catal. Today 28 (1996) 183.
[23] N. Terao, Jpn. J. Appl. Phys. 2 (1963) 156.
[24] P. Griesmar, G. Papin, C. Sanchez, J. Livage, Chem. Mater. 3 (1991) 335.
[25] S.M. Maurer, E.I. Ko, J. Catal. 135 (1992) 125.
[26] G.R. Lee, J.A. Crayston, Adv. Mater. 5 (1993) 434.
[27] B. Ohtani, K. Iwai, S.-I. Nishimoto, T. Inui, J. Electrochem. Soc. 141 (1994) 2439.
[28] E.C. DeCanio, V.P. Nero, E.I. Ko, J. Catal. 146 (1994) 317.
[29] V. Pârvulescu, S. Coman, V.I. Pârvulescu, to be submitted.
[30] D. Nazimek, J. Ryczowski, Appl. Catal. 26 (1986) 47.
[31] G.C. Bond, Chem. Soc. Rev. 20 (1991) 441.
[32] B. Coq, E. Crabb, M. Warawdekar, G.C. Bond, J.C. Slaa, S.

Galvagno, L. Mercadante, J.G. Ruiz, M.C.S. Sierra, J. Mol. Catal. 92 (1994) 107.
[33] G.C. Bond, J.C. Slaa, J. Mol. Catal. A: Chem. 101 (1995) 243.
[34] G.C. Bond, J.C. Slaa, J. Mol. Catal A: Chem. 106 (1996) 135.
[35] G.C. Bond, J.C. Slaa, J. Chem. Technol. Biotechnol. 65 (1996) 15.
[36] J.M. Zowtiak, C.H. Bartholomew, J. Catal. 83 (1983) 107.
[37] R.C. Ruel, C.H. Bartholomew, J. Catal. 85 (1984) 63.
[38] E. Iglesia, S.L. Soled, R.A. Fiato, J. Catal. 137 (1992) 212.
[39] A. Sarkany, Z. Zsoldos, Gy. Stefler, J.W. Hightower, L. Guczi, J. Catal. 157 (1995) 179.
[40] C. de Leitenburg, A. Trovarelli, J. Catal. 156 (1995) 171.
[41] M.A. Stranick, M. Houalla, D.M. Hercules, J. Catal. 103 (1987) 151.
[42] A. Frydman, D.G. Castner, M. Schmal, C.T. Cambell, J. Catal. 152 (1995) 164.
[43] V. Ponec, G.C. Bond, Catalysis by metals and alloy, Stud. Surf. Sci. Catal., Elsevier, Amsterdam, Vol. 95, 1995, p. 284.
[44] H. Yoshitake, K. Asakura, Y. Iwasawa, J. Chem. Soc., Faraday Trans. 85 (1989) 2021.
[45] P. Gallezot, C. Leclercq, J. Barbier, P. Marecot, J. Catal. 116 (1989) 164.
[46] B. Torok, A. Molnar, I. Palinko, M. Bartok, J. Catal. 145 (1994) 295.
[47] B. Torok, I. Palinko, M. Bartok, Catal. Lett. 31 (1995) 421.